

1

Chirality at Metal Surfaces

Chris J. Baddeley and Neville V. Richardson

1.1

Introduction

Since the mid-1990s, the number of surface science investigations of chirality at surfaces has increased exponentially. Advances in the technique of scanning tunneling microscopy (STM) have been crucial in enabling the visualization of single chiral molecules, clusters, and extended arrays. As such, STM has facilitated dramatic advances in the fundamental understanding of the interactions of chiral molecules with surfaces and the phenomena of chiral amplification and chiral recognition. These issues are of considerable technological importance, for example, in the development of heterogeneous catalysts for the production of chiral pharmaceuticals and in the design of biosensors. In addition, the understanding of chirality at surfaces may be a key to unraveling the complexities of the origin of life.

1.1.1

Definition of Chirality

The word chirality is derived from the Greek *kheir* meaning “hand.” It is the geometric property of an object that distinguishes a right hand from a left hand. Lord Kelvin provided a definition of chirality in his 1884 Baltimore Lectures, “I call any geometrical figure or group of points ‘chiral’ and say it has ‘chirality’, if its image in a plane mirror, ideally realized, cannot be brought into coincidence with itself.” For an isolated object, for example, a molecule, the above statement can be interpreted as being equivalent to requiring that the object possesses neither a mirror plane of symmetry nor a point of symmetry (center of inversion). If a molecule possesses either one of these symmetry elements, it can be superimposed on its mirror image and is therefore *achiral*. A chiral molecule and its mirror image are referred to as being a pair of *enantiomers*. Many organic molecules possess the property of chirality. Chiral centers are most commonly associated with the tetrahedral coordination of four different substituents. However, there are many examples of other rigid

structures that have chiral properties where a significant barrier exists to conformational change within the molecule.

1.1.2

Nomenclature of Chirality: The (*R*),(*S*) Convention

Most of the physical properties (e.g., boiling and melting point, density, refractive index, etc.) of two enantiomers are identical. Importantly, however, the two enantiomers interact differently with polarized light. When plane polarized light interacts with a sample of chiral molecules, there is a measurable net rotation of the plane of polarization. Such molecules are said to be optically active. If the chiral compound causes the plane of polarization to rotate in a clockwise (positive) direction as viewed by an observer facing the beam, the compound is said to be dextrorotatory. An anticlockwise (negative) rotation is caused by a levorotatory compound. Dextrorotatory chiral compounds are often given the label D or $(+)$ while levorotatory compounds are denoted by L or $(-)$.

In this chapter, we will use an alternative convention that labels chiral molecules according to their absolute stereochemistry. The (*R*),(*S*) convention or Cahn–Ingold–Prelog system was first introduced by Robert S. Cahn and Sir Christopher K. Ingold (University College, London) in 1951 and later modified by Vlado Prelog (Swiss Federal Institute of Technology) [1]. Essentially, the four atomic substituents at a stereocenter are identified and assigned a priority (1 (highest), 2, 3, 4 (lowest)) by atomic mass. If two atomic substituents are the same, their priority is defined by working outward along the chain of atoms until a point of difference is reached. Using the same considerations of atomic mass, the priority is then assigned at the first point of difference. For example, a $-\text{CH}_2-\text{CH}_3$ substituent has a higher priority than a $-\text{CH}_3$ substituent. Once the priority has been assigned around the stereocenter, the tetrahedral arrangement is viewed along the bond between the central atom and the lowest priority (4) substituent (often a $\text{C}-\text{H}$ bond) from the opposite side to the substituent (Figure 1.1). If the three other substituents are arranged such that the path from 1 to 2 to 3 involves a clockwise rotation, the stereocenter is labeled (*R*) (Latin *rectus* for right). By contrast, if the path involves an anticlockwise rotation, the stereocenter is labeled (*S*) (Latin *sinister* for left). It is important to note that the absolute stereochemistry cannot be predicted from the L or D labels and vice versa.

In nature, a remarkable, and so far unexplained, fact is that the amino acid building blocks of all proteins are exclusively left-handed and that the sugars contained within the double helix structure of DNA are exclusively right-handed. The consequences of the chirality of living organisms are far reaching. The human sense of smell, for example, is able to distinguish between pure (*R*)-limonene (smelling of oranges) and (*S*)-limonene (smelling of lemons). More significantly, two enantiomeric forms of an organic molecule can have different physiological effects on human body. In many cases, one enantiomer is the active component while the opposite enantiomer has no effect (e.g., ibuprofen where the (*S*)-enantiomer is active). However, often the two enantiomers have dramatically different effects. For example, (*S*)-methamphetamine

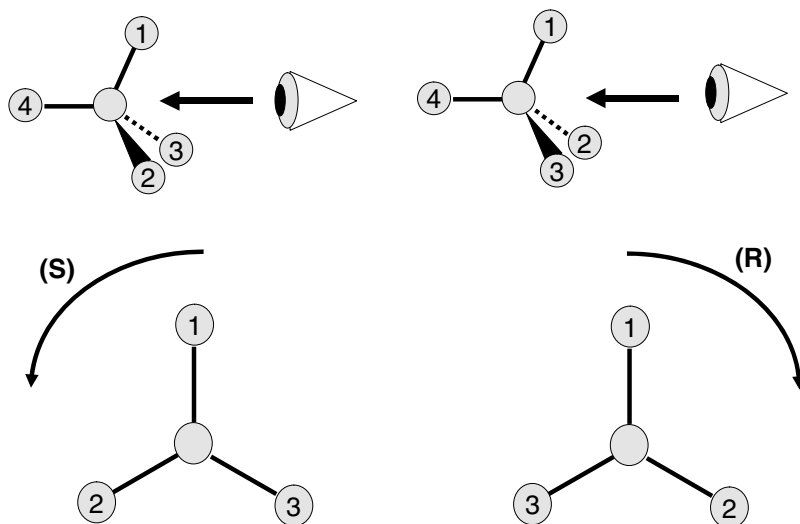


Figure 1.1 Schematic diagram explaining the Cahn-Ingold-Prelog convention for determining the absolute stereochemistry of a chiral molecule.

is a psychostimulant while (*R*)-methamphetamine is the active ingredient in many nasal decongestants (Figure 1.2).

In the pharmaceutical industry, about half of all of the new drugs being tested require the production of exclusively one enantiomeric product. Thermodynamically, this is a challenging problem since the two isolated enantiomers have identical Gibbs energies; the reaction from prochiral reagent to product should therefore result in a 50:50 (*racemic*) mixture at equilibrium. To skew the reaction pathway to form one product with close to 100% enantioselectivity is nontrivial. Knowles [2], Noyori [3], and Sharpless [4] were awarded the Nobel Prize in Chemistry in 2001 for developing enantioselective homogeneous catalysts capable of producing chiral molecules on an industrial scale. Typically, these catalysts consist of organometallic complexes with chiral ligands. Access to the metal center by the reagent is strongly sterically influenced by the chiral ligands resulting in preferential formation of one enantiomeric product. There are many potential advantages of using heterogeneous catalysts, not least the ease of separation of the catalyst from the products. However, despite extensive research over several decades, relatively few successful catalysts have been synthesized on a laboratory scale and the impact on industrial catalysis is essentially negligible. One of the primary motivations behind surface science studies of chirality at surfaces is to understand the surface chemistry underpinning chiral catalysis and to develop methodologies for the rational design of chiral catalysts. Similarly, those interested in issues related to the origin of life are investigating the possibility that surfaces were responsible for the initial seeding of the chiral building blocks of life and that, presumably via some chiral amplification effects, this led to the overwhelming dominance of left-handed amino acids and right-handed sugars in

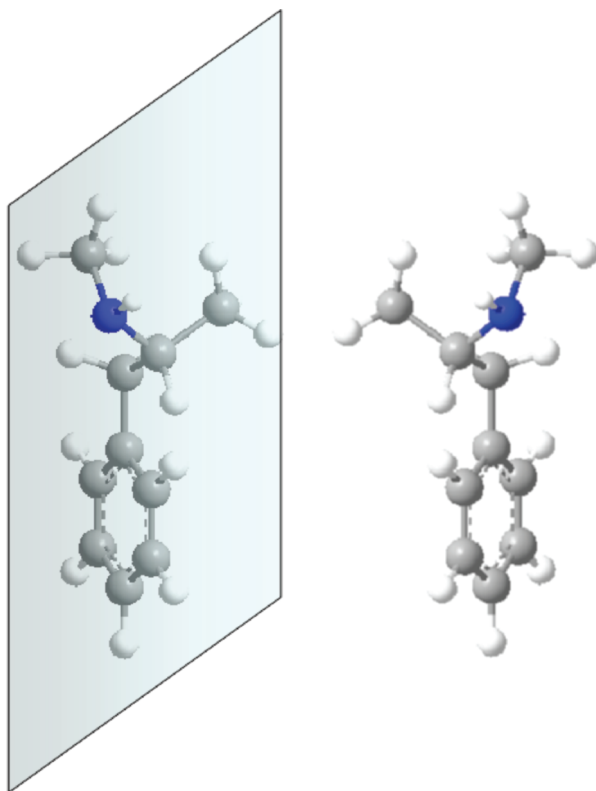


Figure 1.2 The two mirror equivalent forms of the drug methamphetamine. On the right is shown the (*S*)-form of the molecule; on the left is the (*R*)-enantiomer.

biological systems on Earth. As such, the surface chemistry of chiral solids, chiral amplification, and chiral recognition are all important subtopics of chiral surface science. STM has proved to be the single most important tool of researchers in this field.

1.2

Surface Chirality Following Molecular Adsorption

1.2.1

Achiral Molecules on Achiral Surfaces

When a molecule is adsorbed on a surface, the symmetry of the combined adsorbate–substrate system is very likely to be reduced compared to that of the isolated gas-phase species or the bare adsorption site. This raises the possibility that, if mirror planes present in the isolated achiral molecule and those at the relevant

adsorption site of the clean surface are not coincident, then the combined system of a single adsorbed molecule and the substrate will be locally chiral; that is, mirror planes of the isolated molecule are lost on adsorption and chirality is *induced* by the adsorption process. Note that a center of symmetry, also capable of ensuring superimposability of an object and its mirror image, is necessarily incompatible with the presence of a nearby surface [5]. A commonly observed case of such adsorption-induced chirality is that of a planar molecule with C_s symmetry (a single mirror plane) in the gas phase adsorbing on a surface such that the molecular plane is parallel to the substrate, as favored, for example, by van der Waals (vdW) interactions, thereby destroying the mirror plane symmetry. The molecule can then exist in two enantiomeric forms, although necessarily as a racemic mixture in the absence of any other influences that might lead to a preference of one rather than the other. Figure 1.3 illustrates this possibility for 4-[*trans*-2-(pyrid-4-yl-vinyl)]benzoic acid (PVBA) adsorbed parallel to an idealized, unstructured surface [6]

Interconversion of the two enantiomers is possible only if the molecule is removed from the surface and rotated by 180° around an axis parallel to the substrate surface. In the case of PVBA adsorbed on $Ag\{1\ 1\ 1\}$, hydrogen bonding leads to a preference for homochiral double chains based on head-to-tail N–H–O bonds and a C_2 axis relating the two strands of the chains. The chirality of the chain can be recognized in the STM images by the stagger of one strand relative to the other that arises from C–H–O bonds, as shown in Figure 1.3 [6].

The example described above is that of the separation of enantiomers into 1D chains following adsorption-induced chirality. In addition to forming chirally seg-

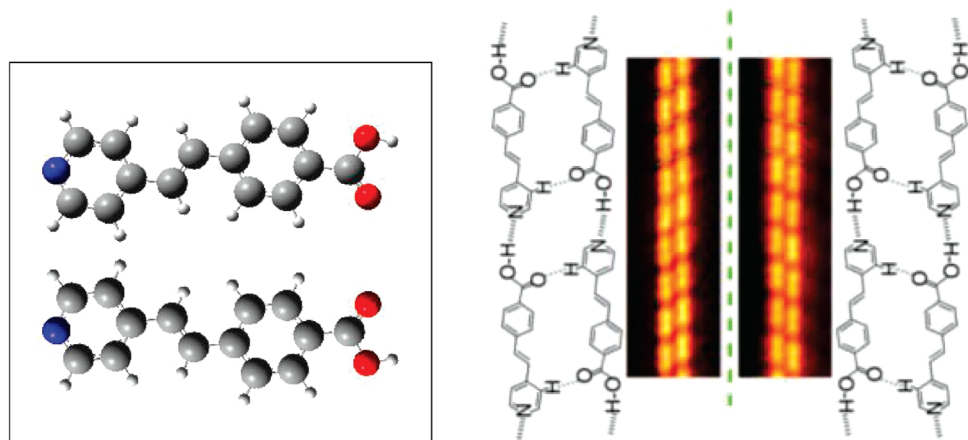


Figure 1.3 Molecular models showing the two enantiomers resulting from the loss of mirror plane symmetry on adsorption with the molecular plane parallel to the substrate. The separation of enantiomers observed by STM is identified by the relative displacement of adjacent monomers within the double chain. (Reprinted with permission from Ref. [6]. Copyright 2001, American Physical Society.)

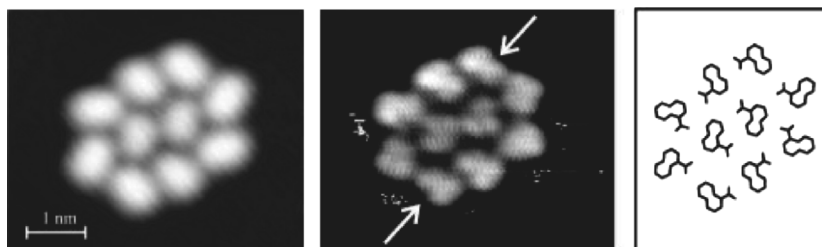


Figure 1.4 Low- and high-resolution STM images of a decamer of 1-nitronaphthalene, together with the minimum structure optimized from a force model, showing individual enantiomers in a 6 : 4 ratio. (Reprinted with permission from Ref. [7]. Copyright 1999, American Physical Society.)

regated chains, 1-nitronaphthalene is able to form chiral decamers [7]. Figure 1.4 shows a cluster of ten 1-nitronaphthalene molecules [8]. The adsorption process on Au {1 1 1} imposes chirality on the molecule and the clusters can be seen to have a pinwheel, chiral conformation, although within the cluster not all the individual molecules have the same handedness. Each cluster contains six molecules of one enantiomer and four of the other. The overall surface is expected to be racemic as regard to both molecules and clusters.

A particularly elegant example of cluster formation involving chiral recognition and retention of chirality through an increasingly complex hierarchical series of clusters is that of rubrene on Au{1 1 1} [9] illustrated in Figure 1.5

The above discussion refers to the loss of mirror symmetry on adsorption leading to chirality at the level of the individual molecule. It is also common for oblique lattices to be formed following molecular adsorption, hence global chirality, even

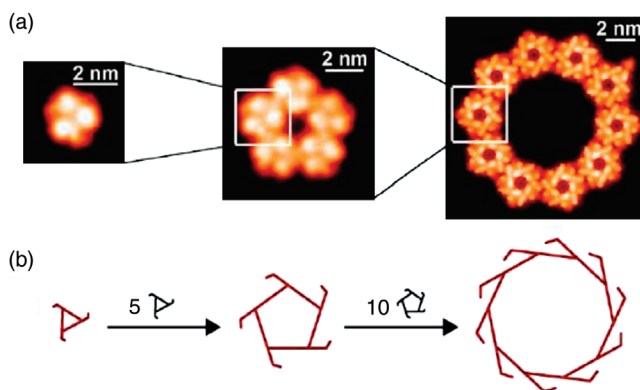


Figure 1.5 (a) Hierarchy of clusters of rubrene on Au{1 1 1}, showing the evolution from trimers to pentamers of trimers and eventually 150 molecules per cluster as a decamer of the pentamers. (b) Illustration of the preservation of chirality through the hierarchy. (Adapted with permission from Ref. [9]).

when the local site retains one or more mirror planes. A specific example of the relationship between local and organizational chirality for a highly symmetric molecule is discussed in some detail in Section 1.2.2.

It is relevant at this point to note that chemistry frequently employs a rather weaker, arguably less precise, definition of chirality than the more “mathematical” definition put forward by Lord Kelvin. A species, which in its most stable conformation has no mirror plane or center of symmetry, is formally chiral but, if there were a low-energy pathway to the enantiomer, for example, by a low-frequency vibrational mode, then, in chemical terminology, this would not normally be considered to be chiral. However, if adsorption of such a species raises the frequency of the vibration substantially, then the energy barrier between the two “enantiomers” may become chemically significant such that the adsorbed molecule is meaningfully described as chiral. An early example of this is the case of the deprotonated glycine species adsorbed on copper surfaces. An isolated glycinate anion, although lacking any mirror plane or center of symmetry, is nevertheless readily converted to its enantiomer principally by a rotation around the C–N bond, with an energy barrier of approximately 35 kJ mol^{-1} , which might readily be overcome at room temperature, such that glycine or glycinate are not generally considered chiral. However, on $\text{Cu}\{110\}$, for example, adsorption takes place through both O atoms and the N atom in a tridentate interaction with the copper surface, each atom in an approximately atop site [10, 11]. This inhibits the interconversion of enantiomers, and surface-induced chirality leads to distinct mirror image species on the surface [12]. Nevertheless, unlike the examples discussed above, segregation of enantiomers into clusters, chains, or arrays does not occur. Instead, one molecule of each enantiomer gives rise to a heterochiral (3×2) unit cell and is interrelated by glide lines as shown in Figure 1.6. This proposal based on LEED, STM, and IR data [10] has been confirmed by photoelectron diffraction [11] and by DFT calculations [13]. A suggestion that a second phase consists of homochiral unit cells [12] has not been confirmed by photoelectron diffraction [11, 14] or theory, although the energy difference of this

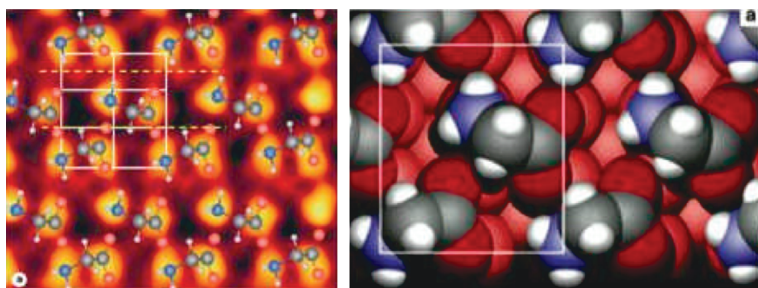


Figure 1.6 The left-hand panel shows a molecular model of the glycinate/ $\text{Cu}\{110\}$ structure with both enantiomers present in the heterochiral (3×2) unit cell, superimposed on an STM image of this surface. (Adapted with permission from Ref. [12]. Copyright 2002,

Elsevier.) The right-hand panel shows the confirmation of this structure calculated by DFT, clearly indicating the atop adsorption sites occupied by the N and both O atoms in this system. (Reprinted with permission from Ref. [13]. Copyright 2004, Elsevier.)

phase is calculated to be small (6 kJ mol^{-1}) [13]. It is likely that the different “phases” imaged by STM [12] result from the two rotational domains of the heterochiral structure appearing distinct because of anisotropy in the tip. Interestingly, intrinsically chiral amino acids such as alanine or phenylglycine can adsorb on the Cu{1 1 0} surface also in a (3×2) structure with an apparent glide line indicated by the LEED pattern, although only a single enantiomer is present [15–17].

1.2.2

Lattice Matching

It would seem inherently unlikely that a highly symmetric (D_{6h}) molecule such as coronene, $C_{24}H_{12}$, could give rise to chiral surfaces and indeed diastereoisomeric interactions, particularly when adsorbed on a hexagonal substrate such as graphite or an fcc{1 1 1} face. Nevertheless, we show in this section that lattice matching between an adsorbate overlayer and the substrate can readily give rise to surface chirality, and while this might be unsurprising in systems of lower symmetry, it is still distinctly likely in adsorbate/substrate systems in which both components have inherently high symmetry. To emphasize this aspect, we choose coronene and a related derivative to illustrate how these effects arise from simple interadsorbate interactions and their simple geometric consequences. To simplify matters further, we restrict the adsorption of coronene and its analogues to atop adsorption sites, where symmetry matching with a hexagonal fcc substrate (also locally D_{6h}) would seem to be optimized.

Nondissociative adsorption of coronene on a late transition or coinage metal is likely to be dominated by van der Waals interactions and rather weak π -d interactions, both of which favor a flat-lying and probably atop adsorption geometry again optimizing the symmetry matching. Although relatively weak, these interactions are strong enough to permit stable monolayers to be formed in UHV at room temperature. Interactions between adsorbed coronene molecules are highly isotropic and again dominated by vdW terms. These, therefore, favor hexagonal close packing in an isolated (no substrate) monolayer of planar coronene molecules. Nevertheless, despite all the apparent symmetry matching, it is the subtle energy balance between interadsorbate interactions and those favoring a specific adsorption site, even an atop one, that gives rise to chiral structures and diastereoisomeric effects.

Coronene (Figure 1.7a), considered as a circle, has a vdW diameter of 11.6 \AA , which corresponds to a molecular area of 105.7 \AA^2 and leads, with hexagonal but non-space filling close packing, to a unit cell area of 116.5 \AA^2 . However, coronene on some hexagonal surfaces has an intermolecular separation somewhat less than 11.6 \AA , for example, 11.27 \AA [18] on graphite and 11.18 \AA on MoS_2 [19], suggesting that it is better considered as having a hexagonal, space filling shape with a vdW width of 11.26 \AA . Even this, however, is insufficient to rationalize the intermolecular separations found on other, admittedly nonhexagonal, surfaces such as Cu{1 0 0} [19] and Cu{1 1 0} [20]. In such systems, intermolecular spacings significantly less than 11 \AA can be found. The explanation, while retaining a flat-lying coronene molecule, since there is no evidence to the contrary, lies in recognizing that the 12 H atoms are almost equally

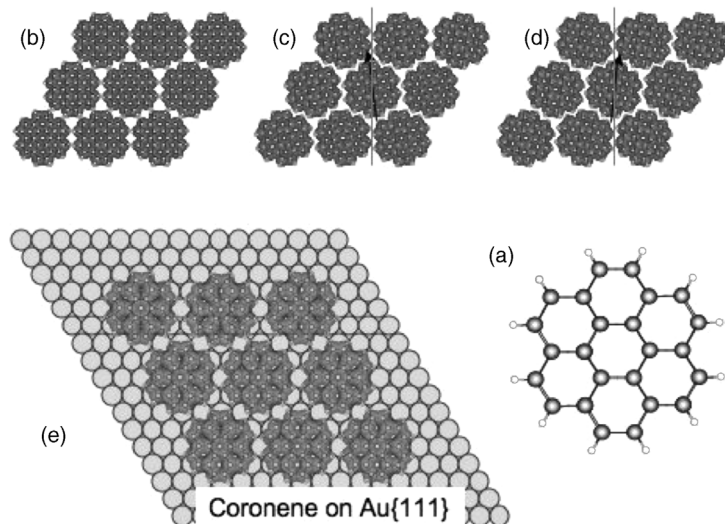


Figure 1.7 (a) Molecular model of coronene; (b) hexagonal close packing at the van der Waals diameter; parts (c) and (d) illustrate the packing advantage, which can be obtained by a concerted rotation, counterclockwise or clockwise, of all molecules to allow interdigitation of the C–H bonds on adjacent molecules; part (e) illustrates the (4×4) model of coronene on Au{111} where the adsorption site dominated separation of molecules is such that interdigitation is unnecessary.

spaced around the periphery of the molecule and confer C_{12} rotational symmetry on the molecule. A concerted rotation of all molecules on the hexagonal lattice by 8.4° about their centers then allows interdigitation of the H atoms on neighboring molecules (Figure 1.7c and d). This permits a 3% reduction of the intermolecular spacing to around 10.9 Å. Herein lies one element of the surface chirality of this molecule.

When the molecules on an isolated hexagonal lattice are rotated in concert away from their initial positions to allow interdigitation and closer packing, the 2D site symmetry is reduced, all mirror planes are lost, and the molecule becomes chiral through the lack of mirror symmetry in the interactions with its neighbors. Rotation to the left or right gives energetically equivalent enantiomers.

There is also a second source of chirality when the adsorbate hexagonal lattice is matched with that of the substrate. For a hexagonal substrate, characterized by unit cell vectors \mathbf{a}_1 and \mathbf{a}_2 aligned along close-packed directions, at 120° to each other and of length a , there are larger hexagonal unit cells defined by unit cell vectors \mathbf{b}_1 and \mathbf{b}_2 , where $\mathbf{b}_1 = m\mathbf{a}_1 + n\mathbf{a}_2$ and $\mathbf{b}_2 = -n\mathbf{a}_1 + (m - n)\mathbf{a}_2$ with m and n integers. These have lengths $b = a\sqrt{(m^2 - mn + n^2)}$ and are rotated $\theta = \tan^{-1}(\sqrt{3}n/(2m - n))$ relative to the substrate unit cell vectors. Many of the smaller ones, based on m and n values up to 6, are familiar overlayers for atomic and molecular adsorbates on fcc{111} substrates, for example, $(\sqrt{3} \times \sqrt{3})R30^\circ$, $(\sqrt{7} \times \sqrt{7})R19.1^\circ$, and so on. For those overlayers where $m = 0$, n , or $2n$, corresponding to rotations of 0° , 60° , and 30° ,

respectively, the structure is achiral since a mirror plane is retained along either the $(1\ 1\ 0)$ or the $(2\ 1\ 1)$ direction. Conversely, if this condition is not met, there is no coincidence of mirror planes between the substrate and overlayer lattices: enantiomeric structures will exist, for example, based on m , n being 3, 1 or 3, 2, that is, $(\sqrt{7} \times \sqrt{7})R19.1^\circ$ and $(\sqrt{7} \times \sqrt{7})R40.9^\circ$, respectively, or perhaps more helpfully described as $(\sqrt{7} \times \sqrt{7})R \pm 19.1^\circ$. Lattice matching of this type giving rise to chiral lattices is common in overlayers on hexagonal substrates, such as the pinwheel structure found for Pd on (1×2) reconstructed $\text{TiO}_2\{1\ 1\ 0\}$ surfaces [21].

In the case of coronene adsorbed on either $\text{Ag}\{1\ 1\ 1\}$ [22] or $\text{Au}\{1\ 1\ 1\}$ [23, 24], an achiral (4×4) structure is observed (Figure 1.7e). This is perhaps unsurprising since this is the hexagonal superlattice that, with a lattice vector of approximately 11.5 Å, is the closest match to the coronene dimensions. Although this lattice is achiral, it demonstrates that the balance between interadsorbate interactions and those favoring a specific adsorption site and hence a commensurate overlayer is important. In contrast, for adsorption of coronene on $\text{Cu}\{1\ 1\ 1\}$, a chiral lattice is predicted based on either $(\sqrt{19} \times \sqrt{19})R \pm 23.4^\circ$ or $(\sqrt{21} \times \sqrt{21})R \pm 10.9^\circ$ lattices. The latter with a unit cell vector of length 11.7 Å might be favored if site preference is strong relative to intermolecular close packing but would not require the concerted rotation of coronene molecules to reduce the intermolecular separation since this is below even the circular diameter of coronene (11.6 Å). Chirality would be limited to that derived solely from the lattice matching and molecules would be free to adopt whatever rotation optimized the energy based on an atop local site geometry. Of course, a twist away from a high-symmetry azimuthal orientation, which might be clockwise or anticlockwise, introduces a second chiral element and hence the need to consider diastereoisomerism. There are four possible choices of lattice/molecular twist that might conveniently be designated $+ / +$, $- / -$ for one pair of enantiomers and $+ / -$, $- / +$ for the other pair. In principle, a particular sense of rotation could favor a particular lattice orientation such that one pair is energetically more favorable than the other. However, since intermolecular interactions are likely to be weak at this separation, the energy difference is likely to be small. This contrasts with the situation if the former lattice, $(\sqrt{19} \times \sqrt{19})R \pm 23.4^\circ$, were preferred because of the importance of intermolecular interactions. In this case, since the substrate imposed lattice dimension is only 11.14 Å, molecular rotation imposed within the 2D adsorbate lattice is required, with C–H interdigitation to achieve this reduced separation as shown in Figure 1.8. The second element of chirality is again a molecular rotation but one that has its origin in the intermolecular interactions rather than molecule–substrate site interactions. The energy preference between the two diastereoisomer pairs is now dictated by which pair leads to the more favorable orientation of the molecule on the atop adsorption site. Notable, perhaps, is that for one diastereoisomer pair the azimuthal orientation of the molecule with respect to the substrate is such that a local high symmetry is recovered because the lattice rotation of 23° , combined with the optimum interdigitation rotation of 8° , realigns the mirror planes of the molecule very closely ($<2^\circ$) with those of the substrate. To our knowledge, coronene adsorption on $\text{Cu}\{1\ 1\ 1\}$ has not been studied, but clearly this system would provide an interesting model for investigating the subtle energy

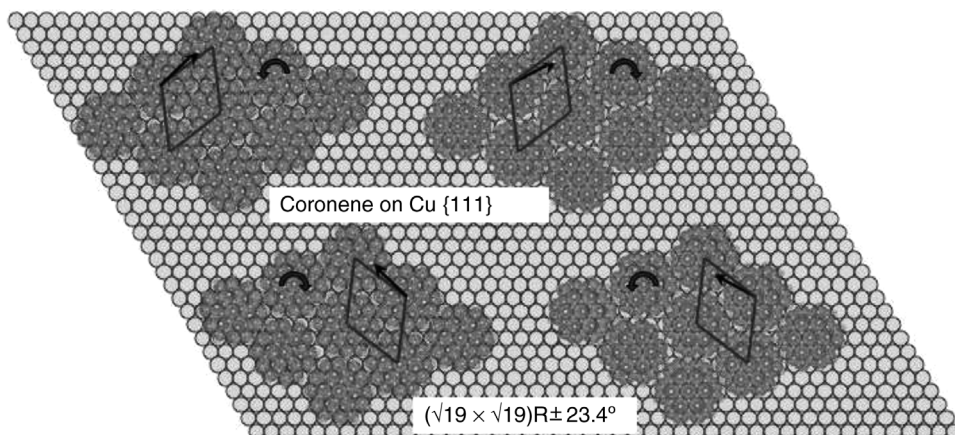


Figure 1.8 Diastereoisomeric effects predicted to arise for coronene adsorption on Cu{1 1 1} from a combination of molecular rotation (curved arrows) within the 2D adsorbate lattice to allow C–H bond interdigitation and the $(\sqrt{19} \times \sqrt{19})R \pm 23.4^\circ$ lattice. The black arrows indicate a high symmetry within the molecule bisecting C–H bonds.

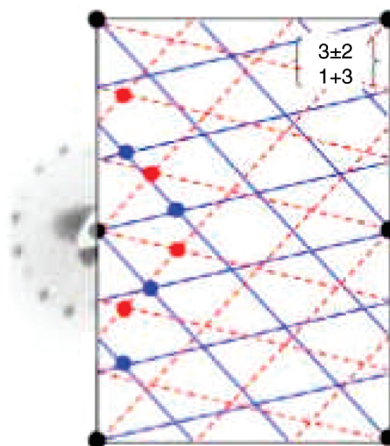
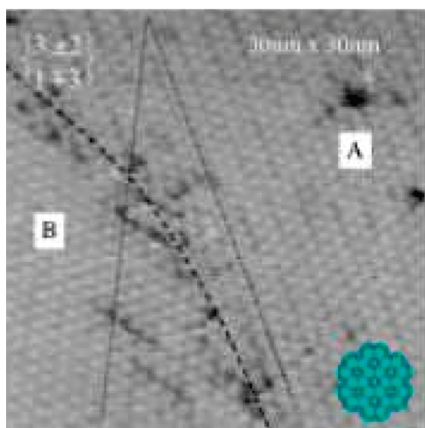


Figure 1.9 UHV-STM image of coronene adsorbed on Cu{1 1 0} showing the two mirror domains A and B. On the right, the LEED pattern showing the contribution of the mirror domains. (Adapted with permission from Ref. [20]. Copyright 2007, IOP Publishing Ltd and Deutsche Physikalische Gesellschaft.)

balance between coronene/coronene interactions and those determining coronene orientation on an atop site.

On fcc {1 1 0} and {1 0 0} surfaces, pseudo-hexagonal lattices can be found [25]. Coronene adsorption on Cu{1 1 0} leads to a $\langle 3 \ 2 \ | \ 1 \ 3 \rangle$ structure and its enantiomer $\langle 3 \ 2 \ | \ 1 -3 \rangle$, shown in Figure 1.9, corresponding to a pseudo-hexagonal lattice with

nearest-neighbor distances of $\sqrt{17a}$, $\sqrt{18a}$, and $\sqrt{19a}$. Interestingly, it is predicted that the distortion to a pseudo-hexagonal lattice creates a second element of chirality in the isolated adsorbate monolayer along with the rotation of the molecule that allows interdigitation. Two diastereoisomer pairs therefore exist within this monolayer even in the absence of the substrate due to the coupling of the two possible directions of rotation and the sense of the sequence of distortions around the hexagon, although of course it is not strictly independent of the substrate since it is the mapping onto the substrate that determines this sequence and the mirror lattice has the mirror sequence of distortion. On Cu{1 0 0}, the structure of adsorbed coronene was originally suggested to be rotational, achiral domains of $p(4 \times 7)$, but that would require an extremely short intermolecular separation of 10.2 Å and a very small unit cell of only 91.4 Å [2, 19]. A more likely interpretation of the LEED is that the structure corresponds to the pseudo-hexagonal, but still achiral, lattice with nearest neighbors at $\sqrt{17a}$, $\sqrt{17a}$, and $\sqrt{18a}$ [25].

The most well-characterized example of the interplay between these various chiral elements, which can arise in molecular adsorption in a constrained pseudo-hexagonal lattice, is that of 2,5,8,11,14,17-hexa-*tert*-butylhexabenzob[bc,ef,hi,kl,no,qr]coronene (HtB-HBC), on Cu{1 1 0} [26]. HtB-HBC is a larger derivative of coronene with a further sequence of aromatic rings around a coronene core and six *t*-butyl substituents instead of hydrogen on the outer periphery. The molecule has a shape close to that of a six-pointed star and gives greater scope for close packing through interdigitation of the *t*-butyl groups by rotation on a hexagonal or pseudo-hexagonal lattice. Elegant, high-resolution STM studies by Schrock *et al.* [26] reveal a $\langle 7\ 2\ | -1\ -5 \rangle$ termed L lattice and mirror image $\langle 7\ -2\ | -1\ 5 \rangle$ R lattice, which are pseudo-hexagonal and exactly $\sqrt{3}$ times larger than the coronene lattice at $\sqrt{51a}$, $\sqrt{54a}$, and $\sqrt{57a}$ as the distorted hexagonal nearest neighbors. These dimensions demand a clockwise or anticlockwise rotation of the molecules on a 2D isolated pseudo-hexagonal lattice to avoid overlap of the vdW envelopes and, when this is mapped onto the substrate R or L lattices, diastereoisomerism results (see Figure 1.10). For the observed pair of enantiomers, the molecules find themselves rotated by $\pm 5^\circ$ relative to the close-packed $\langle 1\ 1\ 0 \rangle$ direction of the substrate, while for the alternative pairing, which is not favored, a rotation by an equivalent amount but in the opposite sense relative to the hexagonal unit cell results in $\pm 21^\circ$ rotation relative to the $\langle 1\ 1\ 0 \rangle$ direction. Studies of an isolated molecule adsorbed on Cu{1 1 1} favor the 5° rotation rationalizing the observed behavior [26]. More detailed discussion of chirality and diastereoisomerism in this system can be found in the paper by Schrock *et al.* [26] and in the work of Richardson [25], where consideration is also given to an alternative chiral structure for HtB-HBC/Cu{1 1 0}, which differs from that observed by Schrock *et al.* [26] only in the orientation of the pseudo-hexagonal lattice to the substrate.

1.2.3

Chiral Molecules on Achiral Surfaces

An isolated molecule, which is chiral in the gas phases, will necessarily be chiral on adsorption if the basic structure and conformation of the molecule are retained.

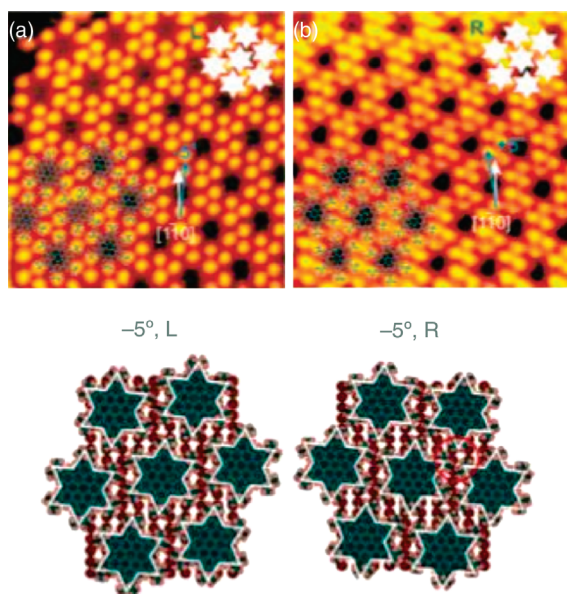


Figure 1.10 UHV-STM images of HtB-HBC adsorption on Cu{1 1 0} showing the correlation between the orientation of the adsorbate lattice vectors and the local rotation of the molecule away from its high symmetry azimuthal orientation atop a copper atom.

The -5° , L ($+5^\circ$, R) gives an improved interdigitation of *t*-butyl groups compared to the diastereoisomers $+5^\circ$, L (-5° , R). (Reprinted with permission from Ref. [25]. Copyright 2006, American Chemical Society.

Adsorption of the opposite gas-phase enantiomer is necessary to generate the mirror image adsorbate system. STM has been widely used to investigate how substrate-mediated interactions and intermolecular hydrogen bonding influence the growth of 1D and 2D clusters and long-range ordered structures. In many cases, if chiral molecules form ordered structures on metal surfaces, the adsorbate forms an oblique unit cell such that the ordered adsorbate structure itself is chiral. In this case, the surface possesses both local chirality (determined by the molecule–surface complex) and global chirality (determined by the chirality of the ordered adsorbate domains).

One of the most extensively studied examples of the adsorption of a simple chiral molecule on an achiral metal surface involves the adsorption of tartaric acid onto Cu {1 1 0}. Tartaric acid (H_2TA) ($\text{HOOC}^*\text{CHOH}^*\text{CHOHCOOH}$) can exist in the (*R,R*), (*S,S*), and (*R,S*) forms. The initial work was motivated by a desire to understand why (*R,R*)-tartaric acid is the most successful chiral modifier in the Ni-catalyzed enantioselective hydrogenation of β -ketoesters. Work from the catalysis community had proposed that ordered, nanoporous 2D arrays of chiral molecules may be important in defining the active site for chiral catalytic reactions [27]. The shape of the chiral nanopores could favor the adsorption of a reactant molecule in a geometry favoring the production of one enantiomeric product. Alternatively, it was proposed that a direct interaction between a prochiral reagent and a single chiral modifier may be

sufficient to direct the reaction along one enantiomeric route [28]. Hence, it was important to investigate how tartaric acid binds to a metal surface and the extent to which it forms ordered 2D arrays. On Cu{1 1 0}, a range of ordered structures were identified with STM following (*R,R*)-tartaric acid adsorption [29] as functions of tartaric acid coverage and temperature. At 300 K and above, tartaric acid adsorption occurred via deprotonation of either one or both $-\text{COOH}$ functionalities to produce monotartrate (HTA) or bitartrate (TA) species. Some of the ordered structures gave unit cells such as $c(4 \times 6)$ that would be indistinguishable from that produced by (*S,S*)-tartaric acid. The $\langle 9\ 0\ | 1\ 2 \rangle$ structure was particularly significant from the point of view of surface chirality. This structure was observed exclusively, with no evidence being found for the mirror image structure $\langle 9\ 0\ | -1\ 2 \rangle$. By contrast, the adsorption of (*S,S*)-tartaric acid gave only the $\langle 9\ 0\ | -1\ 2 \rangle$ structure under similar preparation conditions (Figure 1.11) [30]. In these structures, tartaric acid is adsorbed across the troughs of the Cu{1 1 0} surface in the doubly deprotonated bitartrate form. Barbosa and Sautet used DFT calculations to examine the preference by one enantiomer to form one of the two mirror equivalent domains [31]. It was found that there is an approximately 10 kJ mol^{-1} preference for one ordered arrangement over the other. The energy preference is believed to be derived from an optimization of intramolecular H-bonding interactions involving the two $-\text{OH}$ groups at the chiral centers and was not believed to be related to intermolecular H-bonding interactions since adjacent molecular species are too far apart for any significant H-bonding interactions to occur. Fasel *et al.* carried out a detailed XPD characterization of the adsorption

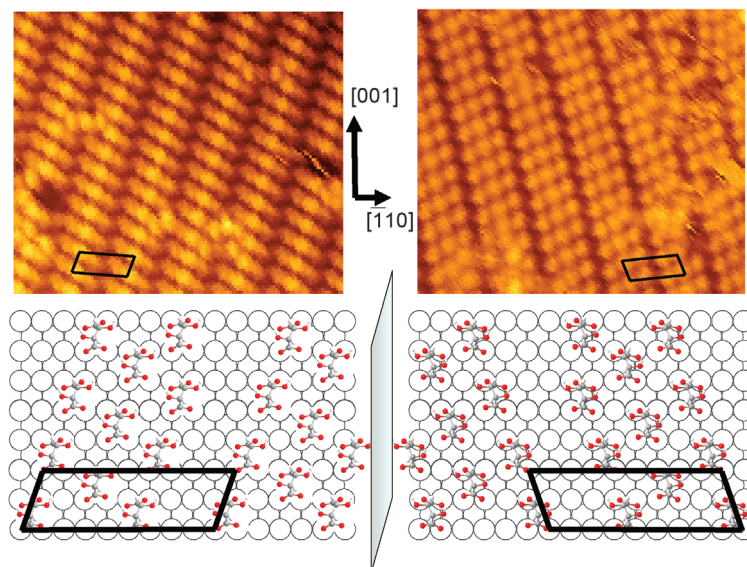


Figure 1.11 STM images ($13.5\text{ nm} \times 11.5\text{ nm}$) of the $\langle 9\ 0\ | 1\ 2 \rangle$ (left) and $\langle 9\ 0\ | -1\ 2 \rangle$ (right) phases of (*R,R*)- and (*S,S*)-tartaric acid, respectively, on Cu{1 1 0}. (Adapted with permission from Ref. [29]. Copyright 2000, Macmillan Publishers Ltd.)

geometry of (*R,R*)- and (*S,S*)-tartaric acid in the $\langle 90 | \pm 1 2 \rangle$ phase and concluded that individual TA species were adsorbed with the planes defined by the two carboxylate OCO planes of each TA species being distorted away from the $\langle -1 1 0 \rangle$ azimuth. The distortion observed by (*R,R*)-TA was exactly mirrored for (*S,S*)-TA [32]. An interesting feature of the $\langle 90 | \pm 1 2 \rangle$ structure is the tendency for clusters with three molecular features to be observed in the STM images. It is implicitly assumed in the proposed structural models that the adsorption site of each TA species is essentially equivalent. If this was the case, then it is not obvious why TA species from clusters of three species separated by channels in the surface. Under certain tip conditions, the three features of the cluster appear to give different *z*-contrast. This may suggest that the three species are in slightly different adsorption sites and that it is energetically more favorable to have an “empty” channel between rows of clusters than to accommodate an additional TA species in a less favorable adsorption site. There is some evidence from STM images of the Ni{1 1 0}/tartaric acid system that the TA species influence the electronic structure of the underlying Ni in the vicinity of the adsorbed TA species perhaps via some local restructuring of Ni atoms [33, 34]. The formation of clusters and channels in the Cu{1 1 0} experiments may be related to a release of strain in the surface copper atoms. This proposed mechanism is supported by a combined DFT and kinetic Monte Carlo study by Hermse *et al.* [35].

1.2.4

Chiral Molecules on Chiral Surfaces

One of the central features of many geochemical models for the origin of life is the proposal that abiotic processes that select left-handed molecules versus right-handed molecules could occur on the surfaces of chiral minerals [36]. There are many examples of minerals whose bulk structures are intrinsically chiral. The most naturally abundant chiral mineral is quartz (SiO_2) that belongs to the trigonal space group $P3_221$. The structure of quartz contains a helical arrangement of corner-linked SiO_4 tetrahedra. The sense of the helix determines left- or right-handed quartz. In addition, more than 200 chiral metal oxide structures are known [37]. Face-centered cubic metallic elements (e.g., Cu, Ni, Pt, etc.) are intrinsically achiral. However, Gellman and coworkers [38] highlighted that certain surfaces of fcc single crystals are chiral (Figure 1.12). Those surfaces displaying kinked steps with uneven step lengths either side of the kink are not superimposable on their mirror image. They proposed that surfaces could be denoted (*R*) or (*S*) by assessing whether the sequence of microfacets in order of decreasing atomic density $\{1 1 1\} > \{1 0 0\} > \{1 1 0\}$ is clockwise (*R*) or anticlockwise (*S*) about the kink atom. STM imaging of step–kink surfaces such as Cu{6 4 3} show a high degree of atom mobility at the step edges [39]. Sholl *et al.* used DFT simulations to show that naturally chiral metal surfaces retain their net chirality even after their local structure is disrupted by thermal step roughening [40]. More recently, Jenkins and Pratt showed that stepped bcc and hcp surfaces may be chiral in the absence of kinks [41].

It was realized at an early stage that the adsorption of two enantiomers at chiral step–kink sites was likely to occur with slightly different adsorption energies. In

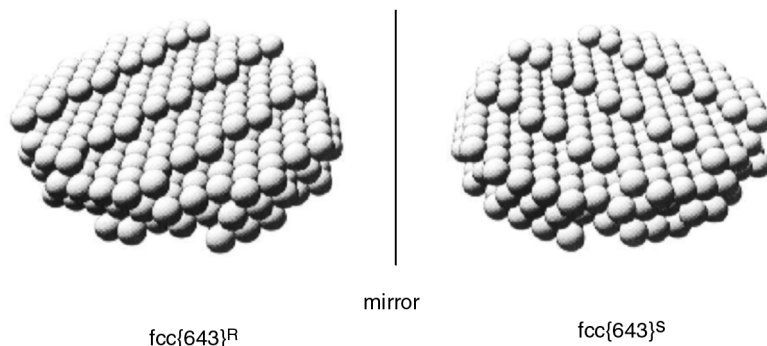


Figure 1.12 Schematic diagram showing the mirror equivalent step-kink arrangements of the fcc $\{6\ 4\ 3\}^R$ and fcc $\{6\ 4\ 3\}^S$ surfaces (Adapted with permission from Ref. [37]. Copyright 1996, American Chemical Society.)

catalysis, such small modifications to the reaction pathway can be amplified to make significant changes in selectivity. Attard, with an elegant series of cyclic voltammetry experiments, displayed not only a difference between the behavior of D- and L-glucose at the (R)-Pt $\{6\ 4\ 3\}$ surface but also an equivalence between the behavior of D-glucose/(R)-Pt $\{6\ 4\ 3\}$ and L-glucose/(S)-Pt $\{6\ 4\ 3\}$ [42]. Temperature-programmed desorption (TPD) has been used to identify subtle differences in adsorption energy for enantiomers at chiral surfaces. For example, Gellman and coworkers reported enantiospecific behavior of (R)- and (S)-propylene oxide on Cu $\{6\ 4\ 3\}$ [43]. However, the adsorption of (R)- and (S)-butanol (the simplest chiral alcohols) produced TPD data that were indistinguishable on Ag $\{6\ 4\ 3\}$ [38].

STM studies of the adsorption of chiral molecules on chiral surfaces are surprisingly sparse. Zhao and Perry showed that (R)-3-methylcyclohexanone forms ordered structures on Cu $\{6\ 4\ 3\}$ with a molecular spacing consistent with the spacing of kinks on the ideal Cu $\{6\ 4\ 3\}$ surface [39]. Kuhnle *et al.* were able to probe, with atomic resolution, the interaction of chiral molecules with kink sites in the case of cysteine on Au $\{1\ 1\ 0\}$ [44]. Although the surface is achiral, it displays both (S)- and (R)-kinks in approximately equal numbers. Kuhnle *et al.* showed that dimers formed from (R)-cysteine adopt different adsorption geometries at (S)-kinks from (S)-cysteine dimers, demonstrating enantiospecific adsorption at these chiral centers. Furthermore, dense, homochiral cysteine islands are found to preferentially grow from kink sites of a specific chirality [44].

1.2.5

Chiral Etching

For an fcc crystal, the low-index faces (e.g., $\{1\ 1\ 1\}$, $\{1\ 0\ 0\}$, and $\{1\ 1\ 0\}$) are thermodynamically the most stable, having the lowest surface free energies.

Chemisorption can lead to large changes in surface free energies. There are many examples where chemisorption of organic molecules on a low-index crystal face results in faceting of a metal surface. A number of factors influence the formation of facets including face-specific adsorption energies, the energy difference between kinks, steps, and terraces, substrate-mediated intermolecular interactions, and surface diffusion barriers. Recent studies of organic molecules adsorbed on low-index surfaces have found that high-index facets can be formed with complex organic molecular adsorbates containing electronegative elements such as O and N atoms in their functional groups. In these systems, the energy gain, which drives the morphology change, could originate from the molecule–substrate interactions and substrate-mediated interadsorbate interactions, which stabilize the steps and kinks of the substrates.

Organic molecules with carboxylic acid functionalities commonly exhibit faceting on metal surfaces. For example, STM investigations have revealed that formic acid [45], benzoic acid [46], and *p*-aminobenzoic acid [47] all exhibit faceting behavior on Cu{1 1 0}. It has been well established that at room temperature the carboxylic acid group is deprotonated to the carboxylate. A preferential alignment of step edges along the [1 1 2] directions can be easily identified for both formate and acetate. It seems likely that the driving force for the formation of this orientation of step edge is the ordering of the molecular species into $c(2 \times 2)$ arrangements. Surface structures formed by the adsorption of benzoic acid are much more complicated [46]. Benzoate species can adopt either flat-lying or upright geometries and may form several different periodic structures depending on coverage and annealing temperature. The related molecule *p*-aminobenzoic acid also displays extensive faceting on the Cu{1 1 0} surface as shown in Figure 1.13 [47]. In these cases, it is possible to identify two symmetrically equivalent (11 13 1) facets giving the characteristic sawtooth arrangement of facets. The fact that similar facets are observed for both benzoic and *p*-aminobenzoic acid leads to the conclusion that the formation of facets is directed by the flat-lying carboxylate units. In the case of formate and acetate, where vibrational spectroscopy reveals upright carboxylate units, step bunching is not observed leading to the proposal that the adsorbate-mediated step–step interaction required for step bunching is at best only weakly attractive when the carboxylate is perpendicular to the surface [48].

Pascual *et al.* [49] investigated the adsorption of the prochiral carboxylic acid 4-*trans*-2-(pyrid-4-yl-vinyl)benzoic acid on Ag{1 1 0}. Following exposure to submonolayer coverages of PVBA and thermal processing, similar sawtooth facets were observed as for benzoic acid on Cu{1 1 0} (Figure 1.14). It was proposed that the formation of facets was driven by the interaction between the carboxylate and the {1 0 0} microfacets at step edges. The microfacets then act as chiral templates nucleating the growth of supramolecular PVBA structures. The chirality of the PVBA species at the microfacet determined the structure of the first four assembled rows of molecules. It is perhaps unsurprising that when a chiral adsorbate is used containing the carboxylate functionality, the distribution of facets produced becomes chiral. Zhao and coworkers carried out studies of the adsorption of a range of amino acids on

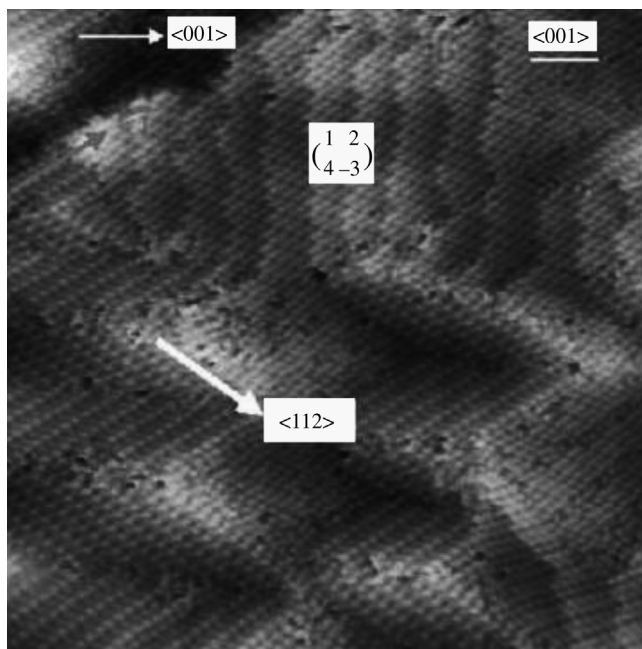


Figure 1.13 High-resolution STM image ($50 \text{ nm} \times 50 \text{ nm}$, bias -1.14 V , tunneling current 6.1 nA) showing the faceted structure of *p*-aminobenzoic acid on $\text{Cu}(1\ 1\ 0)$. (Reprinted with permission from Ref. [47]. Copyright 2003, Elsevier.)

$\text{Cu}\{0\ 0\ 1\}$ [49–52]. In the case of the achiral glycine molecule, a tendency was found for the formation of $(3\ 1\ 17)$ facets. Since there is neither rotational nor reflectional symmetry within individual facets, eight symmetry-related facets should be expected, that is, $(1\ 3\ 17)$, $(1\ 3\ -17)$, $(3\ -1\ 17)$, $(-3\ 1\ 17)$, $(3\ 1\ 17)$, $(3\ 1\ -17)$, $(-1\ 3\ 17)$, and $(1\ -3\ 17)$

The first four facets are rotationally equivalent to each other as are the final four. The two sets are related by reflectional symmetry to each other. When a chiral adsorbate, for example, *S*-lysine, is used, the reflectional symmetry is no longer valid and only rotationally equivalent facets should be formed. This was demonstrated elegantly by Zhao with STM [53]. The driving force for facet formation is proposed to be a “three-point interaction” involving the carboxylate group, the α -amino group, and the amino-terminated side chain. The simultaneous optimization of adsorbate–adsorbate and adsorbate–substrate interactions determines the stereochemistry of the facet.

Surface faceting may be particularly significant in chiral heterogeneous catalysis, particularly in the Ni/β -ketoester system. The adsorption of tartaric acid and glutamic acid onto Ni is known to be corrosive and it is also established that modifiers are leached into solution during both the modification and the catalytic reaction [28]. The preferential formation of chiral step–kink arrangements by corrosive adsorption could lead to catalytically active and enantioselective sites at step–kinks with no requirement for the chiral modifier to be present on the surface.

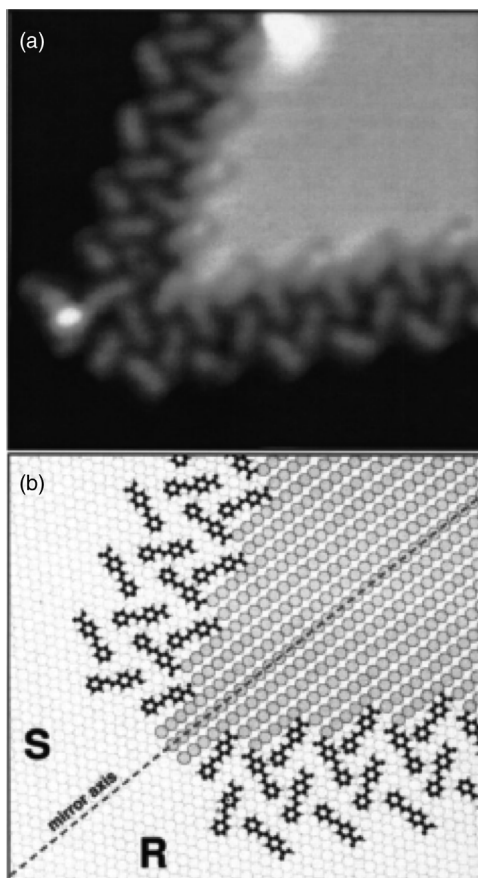


Figure 1.14 (a) STM image ($10\text{ nm} \times 10\text{ nm}$, tip bias $+0.52\text{ V}$, tunneling current 0.5 nA) of a PVBA-induced “sawtooth blade” in a restructured $\text{Ag}(1\ 1\ 0)$ surface terrace. (b) Structural model of the chiral kink arrangements induced by lateral interaction of molecular carboxylate end groups with $\text{Ag}\{1\ 0\ 0\}$ microfacets. (Reprinted with permission from Ref. [48]. Copyright 2004, American Institute of Physics.)

1.3 Chiral Amplification and Recognition

1.3.1 Chiral Amplification in Two Dimensions

In Section 1.2.1, we discussed the phenomenon of adsorbate-induced chirality whereby the adsorption of achiral species (e.g., glycine) results in the formation of two mirror equivalent domains on the surface. It has recently been shown that the presence of relatively small mole fractions of chiral dopants can result in the exclusive

formation of one of the two mirror equivalent domains of the achiral species. For example, succinic acid ($\text{HOOCCH}_2\text{CH}_2\text{COOH}$), an achiral molecule, forms two mirror equivalent domains $\langle 9\ 0\ | -2\ 2 \rangle$ and $\langle 9\ 0\ | 2\ 2 \rangle$ on $\text{Cu}\{1\ 1\ 0\}$ [54]. The doubly deprotonated succinate species are bound via both carboxylate groups to the Cu surface—the mirror relationship between the two domains is thought to arise from the twist of the carbon backbone of succinate with respect to the $[0\ 0\ 1]$ surface direction.

When as little as 2 mol% (*R,R*)-tartaric acid is coadsorbed with succinic acid, LEED beams associated with the $\langle 9\ 0\ | -2\ 2 \rangle$ structure are extinguished. The opposite behavior is observed when the dopant is (*S,S*)-tartaric acid [55]. This behavior is analogous to the “sergeants and soldiers” principle observed for helical polyisocyanate copolymers [56]. The mechanism for this effect is proposed to be substrate-mediated. Succinate species are unable to form intermolecular H-bonds, so a chiral footprint imposed on the surface by a tartrate species is thought to control the adsorption geometry of the surrounding complex creating an effect that is amplified over 30–50 molecules in a given domain [55].

1.3.2

Chiral Switching

In discussing adsorption-induced chirality, it is generally assumed that interconversion of enantiomers is highly unlikely since such an interconversion, for example, under thermal excitation, requires a reduced interaction with the surface and desorption is a more probable outcome. However, if the molecule is relatively large and the chiral center does not make a large contribution to the molecule–substrate binding, then there is the possibility that a low-frequency mode can be excited sufficiently on heating that a bond rotation is possible leading to a chiral switching even without the molecule fully leaving the surface. This effect has been observed by Linderoth and coworkers [57]. The molecule consists of a linear backbone formed out of three benzene rings connected by ethynylene spokes and is functionalized at each end with an aldehyde, a hydroxyl, and a *tert*-butyl group. The molecule is achiral in the gas phase but adsorption on $\text{Au}\{1\ 1\ 1\}$, with the main molecular backbone parallel to the surface, creates, by restricting rotation around the ethynylene spokes, two equivalent chiral centers such that molecules can be classified as LL, RR, or RL, the latter being internally racemic. The *tert*-butyl group can be readily identified in the STM image and its position relative to the molecular backbone determined, thereby permitting the chirality properties of the molecule to be determined. Thermal switching of conformations was noted and ascribed to a partial loss of binding at one end of the molecule. Detailed temperature-dependent studies allowed the barrier to switching to be determined as approximately 0.3 eV. More subtly, it is found that the internally racemic LR/RL conformation has a relatively low probability on the surface and that it is more likely to switch than the LL or RR enantiomers: the difference in barrier heights being 0.04 eV. This is related to the interadsorbate interactions, which favor the LL/RR molecules over LR/RL. The possibility for chiral switching of this type provides a new mechanism for the growth of large homochiral domains as an alternative to separation relying on interdiffusion.

1.3.3

Chiral Recognition

Perhaps the simplest form of chiral recognition is that in which one enantiomer, for example, A, of a chiral object displays a stronger interaction with a particular enantiomer of a second chiral object, for example, B, rather than its mirror image, B*. Of the four possible *diastereoisomeric* interactions AB, A*B*; A*B, AB*, the first two form a mirror equivalent, enantiomeric pair as do the latter. However, the cross-relationships are inequivalent, nonmirror images, for example, AB and AB*, and in a chemical system, there would be an energetic preference for one pair of enantiomers over the other. This is the key to the significance of chirality in biology and, therefore, in the need to develop chiral products in the pharmaceutical and agrochemical industries. Studying chiral recognition processes at surfaces is therefore relevant to a better understanding of the separation of enantiomers, for example, following their preparation in an insufficiently enantioselective reaction. It is also relevant to the development of biosensors and biocompatible materials. We have already covered the interaction of chiral molecules with chiral surfaces, which is an important example of chiral recognition and diastereoisomerism. In this section, attention is focused on chiral recognition between molecules adsorbed on surfaces and it is useful to distinguish between self-recognition processes and those involving different molecular species. The latter can be described by the AB system introduced above while extending the analogy to self-recognition; it is the energy differences between the species AA, A*A*; A*A, AA* that is of interest. Here, AA is the mirror image of A*A*, so these form a pair of enantiomers. Similarly, A*A and AA* are also enantiomers but somewhat trivially since they are also equivalent and might be described as internally racemic.

We have already discussed examples of what is effectively chiral self-recognition, when we described the formation of chiral clusters, chains, and arrays following adsorption involving induced chirality in otherwise achiral species in Section 1.2.1. Now, we show examples of self-recognition between intrinsically chiral molecules adsorbed as a racemic mixture on achiral surfaces leading to segregation of enantiomers if the homochiral (AA/A*A*) pairing is preferred over the heterochiral interaction (AA*). A nice example of this is revealed in the work of Besenbacher and coworkers [58] on the adsorption of a racemic mixture of D- and L-cysteine on Au{1 1 0}. At low coverages, STM shows the molecules are present in pairs and, on the basis of the alignment of any given pair with respect to the $\langle 1\ 1\ 0 \rangle$ direction, it can be identified as being either DD or LL. Notably, DL heterochiral pairs are not observed (Figure 1.15). The reason for the homochiral preference lies in the orientation of the cysteine molecules on the gold surface determined by Au–S and Au–N interactions. The carboxylic acid functionality is not involved in any significant interaction with the gold substrate but rather dominates the pairing interaction between enantiomers. This “three-point” bonding of each molecule, Au–S, Au–N, and O–H–O, drives the self-recognition preference for homochiral pairs [58].

A more subtle example of homochiral preference, which draws attention to the conformational changes in the molecules needed to achieve self-recognition, is that

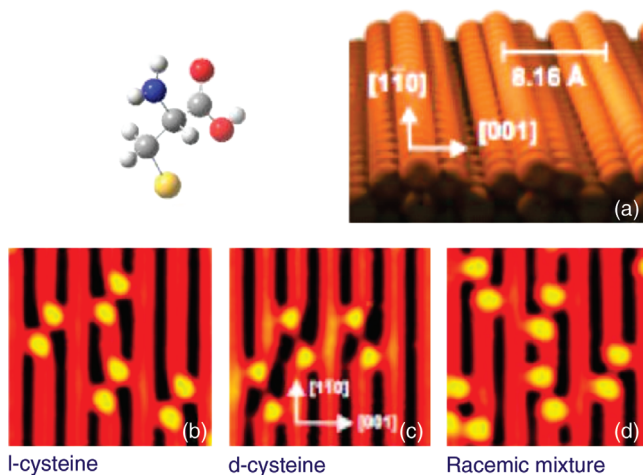


Figure 1.15 Adsorption of cysteine on Au{1 1 0}. Molecular model shows the deprotonated thiolate surface species. (a) Model of the reconstructed (1×2) -Au{1 1 0} surface; (b–d) show, respectively, dimers of L-cysteine, D-cysteine, and the two together characteristically rotated relative to the $\langle 1 1 0 \rangle$ azimuth. (Adapted with permission from Ref. [57]. Copyright 2002, Macmillan Publishers Ltd.)

of the dipeptide D-phenylalanine-D-phenylalanine (D-Phe-D-Phe) and its enantiomer L-Phe-L-Phe adsorption on Cu{1 1 0} [59]. Following adsorption of a racemic mixture at low coverage, isolated species are recognizable by the orientation of their principal axis with respect to the $\langle 1 1 0 \rangle$ azimuth of the substrate; the LL (DD) enantiomer is rotated 34° (counter) clockwise as shown in Figure 1.16. Density functional and molecular dynamics calculations support an interpretation that the molecule adopts a conformation similar to the gas phase, in which the amine and carboxylic acid functionalities lie on the same side of the principal molecular axis, the peptide backbone. In contrast, homochiral chains $(D\text{-Phe-D-Phe})_n$ and $(L\text{-Phe-L-Phe})_n$ are observed by STM to have the principal axis rotated by $\pm 74^\circ$ and heterochiral chains are not observed. Calculations suggest that the conformation of each molecule in a chain is dramatically changed relative to the isolated molecules with, *inter alia*, the amine and carboxylic functionalities now lying on opposite sides of the backbone to optimize intermolecular zwitterion formation between the amine of one molecule and the carboxylic acid of its neighbor. The need to consider the dynamic nature rather than simple lock–key models of chiral recognition is thereby emphasized.

Adenine as an isolated molecule has no symmetry elements and therefore might “mathematically” be considered chiral; however, as in the case of glycine (Section 1.2.1), this description is not useful in chemistry since the enantiomers differ only by inversion through the weakly pyramidal nitrogen atom of the amine functionality, the main body of the molecule being planar. The inversion corresponds to a low-frequency vibration and a low-energy barrier such that single enantiomers

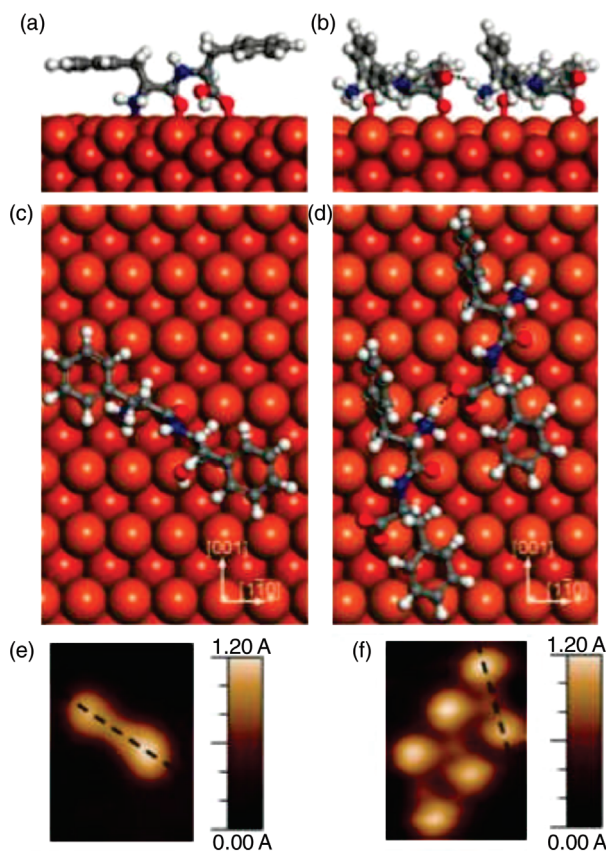


Figure 1.16 Comparison of the structure of an isolated (*L*-Phe-*L*-Phe) on Cu{1 1 0} rotated 34° clockwise with respect to the $\langle 1\ 1\ 0 \rangle$ azimuth (a, c, e) and that of the molecules found in rows that are rotated by 74° (b, d, f) based on STM

images. The superimposed models indicate that the change in rotation is linked to a major change of conformation to enable strong intermolecular bonding. (Adapted with permission from Ref. [58].)

cannot be realized. However, adsorption of adenine on a Cu{1 1 0} surface gives rise to flat-lying molecules, which then have a high barrier to interchange of enantiomers; that is, chirality is induced by adsorption [60]. At coverages up to one monolayer, adenine forms homochiral dimers that link into homochiral chains, whose direction on the Cu{1 1 0} substrate is correlated with their chirality [60] as shown in the left panel of Figure 1.17.

Subsequent adsorption of one enantiomer of phenylglycine leads to an intermolecular recognition process that favors the decoration of chains running in the (1, 2) direction by *S*-phenylglycine (right-hand panel of Figure 1.17) while *R*-phenylglycine decorates the mirror image (1, -2) adenine chains [61]. The origin of the strong interaction between the amino acid, which adsorbs on Cu{1 1 0} as the anion, and the nucleic acid base is electrostatic favoring the close approach of the carboxylate functionality of phenylglycine to the nitrogen of the adenine's amine group, which

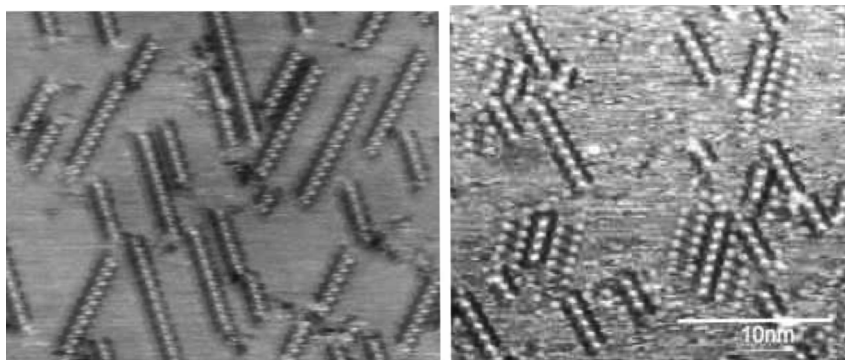


Figure 1.17 The left-hand STM image shows homochiral adenine rows aligned in low symmetry but mirror image azimuths on a Cu(110) surface. On the right, adenine rows in the (1,2) direction are decorated with double rows of *S*-phenylglycine molecules, while no such interaction occurs with (1, -2) rows. (Adapted with permission from Ref. [60]. Copyright 2000, Macmillan Publishers Ltd.)

lies on the periphery of the chain [62]. Chiral recognition occurs because there is also a repulsive interaction between the amine groups of the two molecules and this is less for the favored enantiomer than for the other [62].

1.3.4

Prochiral Molecules Interacting with Chiral Surfaces

In enantioselective catalysis, the key problem to overcome is the fact that the Gibbs energy change from gas-phase prochiral reagent to gas-phase product is identical for each enantiomeric product molecule. Hence, in the absence of any chiral influence on the reaction, a racemic mixture of products should always ensue. By providing a reaction pathway to one product that has a much lower activation barrier, the selectivity can be skewed to give an enantiomeric excess of one product. One of the most heavily researched examples of heterogeneous enantioselective catalysis is the hydrogenation of β -ketoesters over Ni catalysts [28]. The simplest β -ketoester is methylacetoacetate (MAA). This molecule is approximately planar and can adsorb via either molecular face with equal probability. The hydrogenation reaction is believed to occur via dissociative adsorption of H_2 on the metal surface and attack by H from underneath the molecular plane of MAA. The stereochemistry of the chiral center thus produced would be determined by which face of the prochiral reagent lies down on the surface. To skew the reaction in an enantioselective direction, a clear requirement seems to be to restrict the adsorption geometry to exclusively one enantioface. In this respect, the coverage of chiral modifier is thought to be crucial. If the coverage is too low, the formation of 1:1 complexes between modifier and reactant could induce some enantioselectivity, but the adsorption of MAA on bare metal sites would be expected to occur racemically. If the coverage is too high, there

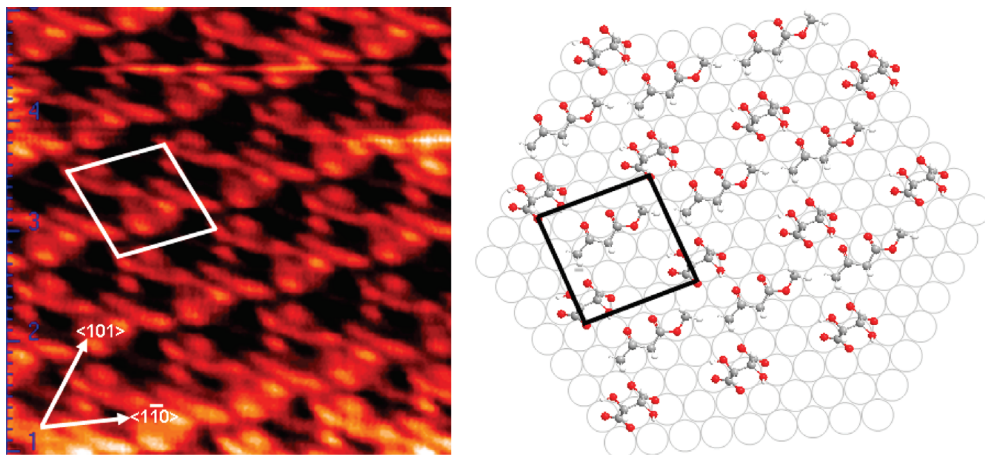


Figure 1.18 STM image ($4 \text{ nm} \times 4 \text{ nm}$) showing the 2D “cocrystalline” structure consisting of an ordered array of 1 : 1 H-bonded complexes of (*R,R*)-tartrate and methylacetoacetate species on $\text{Ni}\{111\}$ giving a chiral $(3\bar{1})-34$ structure. (Adapted with permission from Ref. [62]. Copyright 2002, Elsevier.)

may be insufficient space for MAA to adsorb on the surface. Indeed, the sticking probability of MAA on $\text{Ni}\{111\}$ covered by high coverages of (*R,R*)-tartaric acid [63] or (*S*)-glutamic acid [64] is essentially zero. At intermediate tartaric acid coverages, Jones and Baddeley showed that the adsorption of MAA caused a restructuring of the tartrate adlayer and the formation of an ordered array of 1 : 1 tartrate:MAA complexes (Figure 1.18). Interestingly, the geometry of each MAA molecule in the array appeared identical and corresponding to the geometry required for the formation of (*R*)-methyl-3-hydroxybutyrate – the product observed in excess in the catalytic reactions [63].

1.4 Conclusions

Chirality at surfaces can be manifested in a number of forms including the intrinsic chirality of the surface structure and even the induction of chirality via the adsorption of achiral molecules onto achiral surfaces. The ability of STM to probe surfaces on a local scale with atomic/molecular resolution has revolutionized the understanding of these phenomena. Surfaces that are globally chiral either due to their intrinsic structure or due to the adsorption of chiral molecules have been shown by STM to establish control over the adsorption behavior of prochiral species. This could have profound consequences for the understanding of the origin of homochirality in life on Earth and in the development of new generations of heterogeneous chiral catalysts that may, finally, make a substantial impact on the pharmaceutical industry.

References

- 1 Cahn, R.S., Ingold, C.K., and Prelog, V. (1966) *Angew. Chem. Int. Ed. Engl.*, **78**, 385.
- 2 Knowles, W.S. (2002) *Angew. Chem. Int. Ed.*, **41**, 1999.
- 3 Noyori, R. (2002) *Angew. Chem. Int. Ed.*, **41**, 2008.
- 4 Sharpless, K.B. (2002) *Angew. Chem. Int. Ed.*, **41**, 2024.
- 5 Bradshaw, A.M. and Richardson, N.V. (1996) *Pure Appl. Chem.*, **68**, 457.
- 6 Weckesser, J., De Vita, A., Barth, J.V., Cai, C., and Kern, K. (2001) *Phys. Rev. Lett.*, **87**, 096101.
- 7 Bohringer, M., Morgenstern, K., Schneider, W.D., Berndt, R., Mauri, F., De Vita, A., and Car, R. (1999) *Phys. Rev. Lett.*, **83**, 324.
- 8 Bohringer, M., Morgenstern, K., Schneider, W.D., and Berndt, R. (1999) *Angew. Chem. Int. Ed.*, **38**, 821.
- 9 Blum, M.C., Cavar, E., Pivetta, M., Patthey, F., and Schneider, W.D. (2005) *Angew. Chem. Int. Ed.*, **44**, 5334.
- 10 Barlow, S.M., Kitching, K.J., Haq, S., and Richardson, N.V. (1998) *Surf. Sci.*, **401**, 322.
- 11 Booth, N.A., Woodruff, D.P., Schaff, O., Giessel, T., Lindsay, R., Baumgartel, P., and Bradshaw, A.M. (1998) *Surf. Sci.*, **397**, 258.
- 12 Chen, Q., Frankel, D.J., and Richardson, N.V. (2002) *Surf. Sci.*, **497**, 37.
- 13 Rankin, R.B. and Sholl, D.S. (2004) *Surf. Sci.*, **548**, 301.
- 14 Toomes, R.L., Kang, J.H., Woodruff, D.P., Polcik, M., Kittel, M., and Hoefl, J.T. (2003) *Surf. Sci.*, **522**, L9.
- 15 Haq, S., Massey, A., Moslemzadeh, N., Robin, A., Barlow, S.M., and Raval, R. (2007) *Langmuir*, **23**, 10694.
- 16 Sayago, D.I., Polcik, M., Nisbet, G., Lamont, C.L.A., and Woodruff, D.P. (2005) *Surf. Sci.*, **590**, 76.
- 17 Rankin, R.B. and Sholl, D.S. (2005) *Surf. Sci.*, **574**, L1.
- 18 Lackinger, M., Griessl, S., Heckl, W.M., and Hietschold, M. (2002) *Anal. Bioanal. Chem.*, **374**, 685.
- 19 England, C.D., Collins, G.E., Schuerlein, T.J., and Armstrong, N.R. (1994) *Interfac. Des. Chem. Sensing*, **561**, 202.
- 20 Richardson, N.V. (2007) *New J. Phys.*, **9**, 395.
- 21 Bennett, R.A., Pang, C.L., Perkins, N., Smith, R.D., Morrall, P., Kvon, R.I., and Bowker, M. (2002) *J. Phys. Chem. B*, **106**, 4688.
- 22 Lackinger, M., Griessl, S., Heckl, W.M., and Hietschold, M. (2002) *J. Phys. Chem. B*, **106**, 4482.
- 23 Gyarfás, B.J., Wiggins, B., Zosel, M., and Hippias, K.W. (2005) *Langmuir*, **21**, 919.
- 24 Yoshimoto, S., Narita, R., and Itaya, K. (2002) *Chem. Lett.*, 356.
- 25 Richardson, N.V. (2007) *New J. Phys.*, **9**, 395.
- 26 Schrock, M., Otero, R., Stojkovic, S., Hummelink, F., Gourdon, A., Laegsgaard, E., Stensgaard, I., Joachim, C., and Besenbacher, F. (2006) *J. Phys. Chem. B*, **110**, 12835.
- 27 Webb, G. and Wells, P.B. (1992) *Catal. Today*, **12**, 319.
- 28 Izumi, Y. (1983) *Adv. Catal.*, **32**, 215.
- 29 Lorenzo, M.O., Haq, S., Bertrams, T., Murray, P., Raval, R., and Baddeley, C.J. (1999) *J. Phys. Chem. B*, **103**, 10661.
- 30 Lorenzo, M.O., Baddeley, C.J., Muryn, C., and Raval, R. (2000) *Nature*, **404**, 376.
- 31 Barbosa, L. and Sautet, P. (2001) *J. Am. Chem. Soc.*, **123**, 6639.
- 32 Fasel, R., Wider, J., Quitmann, C., Ernst, K.H., and Greber, T. (2004) *Angew. Chem. Int. Ed.*, **43**, 2853.
- 33 Humblot, V., Haq, S., Muryn, C., Hofer, W.A., and Raval, R. (2002) *J. Am. Chem. Soc.*, **124**, 503.
- 34 Hofer, W.A., Humblot, V., and Raval, R. (2004) *Surf. Sci.*, **554**, 141.
- 35 Hermse, C.G.M., van Bavel, A.P., Jansen, A.P.J., Barbosa, L., Sautet, P., and van Santen, R.A. (2004) *J. Phys. Chem. B*, **108**, 11035.

- 36 Hazen, R.M. and Sholl, D.S. (2003) *Nat. Mater.*, **2**, 367.
- 37 Halasyamani, P.S. and Poeppelmeier, K.R. (1998) *Chem. Mater.*, **10**, 2753.
- 38 McFadden, C.F., Cremer, P.S., and Gellman, A.J. (1996) *Langmuir*, **12**, 2483.
- 39 Zhao, X.Y. and Perry, S.S. (2004) *J. Mol. Catal. A – Chem.*, **216**, 257.
- 40 Sholl, D.S., Asthagiri, A., and Power, T.D. (2001) *J. Phys. Chem. B*, **105**, 4771.
- 41 Jenkins, S.J. and Pratt, S.J. (2007) *Surf. Sci. Rep.*, **62**, 373.
- 42 Attard, G.A. (2001) *J. Phys. Chem. B*, **105**, 3158.
- 43 Horvath, J.D. and Gellman, A.J. (2001) *J. Am. Chem. Soc.*, **123**, 7953.
- 44 Kuhnle, A., Linderoth, T.R., and Besenbacher, F. (2006) *J. Am. Chem. Soc.*, **128**, 1076.
- 45 Bowker, M., Poulston, S., Bennett, R.A., and Stone, P. (1998) *J. Phys. Condens. Matter*, **10**, 7713.
- 46 Chen, Q., Perry, C.C., Frederick, B.G., Murray, P.W., Haq, S., and Richardson, N.V. (2000) *Surf. Sci.*, **446**, 63.
- 47 Chen, Q., Frankel, D.J., and Richardson, N.V. (2001) *Langmuir*, **17**, 8276.
- 48 Chen, Q. and Richardson, N.V. (2003) *Prog. Surf. Sci.*, **73**, 59.
- 49 Pascual, J.I., Barth, J.V., Ceballos, G., Trimarchi, G., De Vita, A., Kern, K., and Rust, H.P. (2004) *J. Chem. Phys.*, **120**, 11367.
- 50 Zhao, X.Y., Gai, Z., Zhao, R.G., Yang, W.S., and Sakurai, T. (1999) *Surf. Sci.*, **424**, L347.
- 51 Wang, H., Zhao, X.Y., and Yang, W.S. (2000) *Acta Phys. Sin.*, **49**, 1316.
- 52 Wang, H., Zhao, X.Y., Zhao, R.G., and Yang, W.S. (2001) *Chin. Phys. Lett.*, **18**, 445.
- 53 Zhao, X.Y. (2000) *J. Am. Chem. Soc.*, **122**, 12584.
- 54 Humblot, V., Lorenzo, M.O., Baddeley, C.J., Haq, S., and Raval, R. (2004) *J. Am. Chem. Soc.*, **126**, 6460.
- 55 Parschau, M., Romer, S., and Ernst, K.H. (2004) *J. Am. Chem. Soc.*, **126**, 15398.
- 56 Green, M.M., Reidy, M.P., Johnson, R.J., Darling, G., Oleary, D.J., and Willson, G. (1989) *J. Am. Chem. Soc.*, **111**, 6452.
- 57 Weigelt, S., Busse, C., Petersen, L., Rauls, E., Hammer, B., Gothelf, K.V., Besenbacher, F., and Linderoth, T.R. (2006) *Nat. Mater.*, **5**, 112.
- 58 Kuhnle, A., Linderoth, T.R., Hammer, B., and Besenbacher, F. (2002) *Nature*, **415**, 891.
- 59 Lingensfelder, M., Tomba, G., Costantini, G., Ciacchi, L.C., De Vita, A., and Kern, K. (2007) *Angew. Chem. Int. Ed.*, **46**, 4492.
- 60 Chen, Q., Frankel, D.J., and Richardson, N.V. (2002) *Langmuir*, **18**, 3219.
- 61 Chen, Q. and Richardson, N.V. (2003) *Nat. Mater.*, **2**, 324.
- 62 Blankenburg, S. and Schmidt, W.G. (2007) *Phys. Rev. Lett.*, **99**, 196107.
- 63 Jones, T.E. and Baddeley, C.J. (2002) *Surf. Sci.*, **519**, 237.
- 64 Jones, T.E., Urquhart, M.E., and Baddeley, C.J. (2005) *Surf. Sci.*, **587**, 69.

